PROCEEDINGS of the
23rd International Congress on Acoustics
9 to 13 September 2019 in Aachen, Germany

# Numerical investigation of the reverberation method for measuring the total loss factor of plate-like structures

Yasutomo YAMASAKI[(1)], Naohisa INOUE[(2)], Tetsuya SAKUMA[(3)]

[(1)]Graduate School of Frontier Sciences, The University of Tokyo, Japan, 2835299483@edu.k.u-tokyo.ac.jp
[(2)]ditto, Japan, n-inoue@edu.k.u-tokyo.ac.jp
[(3)]ditto, Japan, sakuma@e.u-tokyo.ac.jp

**Abstract**

The total loss factor measurement by the reverberation method is often performed to estimate the boundary conditions of vibration fields of plate-like structures. In order to clarify how measured values involve discrepancies from the true values, this paper presents a numerical model that simulates the reverberation method to determine the loss factor in a bending vibration system of a glass plate supported with an elastic material. As a reference, the total loss factor of a finite plate system is theoretically calculated based on the diffuse vibration field assumption, where the random-incidence vibration absorption coefficient on the support edge is given for the semi-infinite plate terminated by the mechanical and moment impedances. Subsequently, the finite element analysis is performed for a rectangular plate with the impedance boundary, and impulse responses are calculated with different arrangements of excitation and receiving points. Comparing the theoretical and numerical results, the validity of the measurement procedures is generally confirmed, however, it is demonstrated that the measured loss factors tend to become slightly higher than theoretical ones. Additionally, measured results on real window systems are discussed briefly.

Keywords: Thin plate, Finite element method, Loss factor

## 1 INTRODUCTION

Understanding vibro-acoustical behaviors of plate-like structures are of great interest in many fields of noise control engineering. Regarding the acoustic radiation from a rectangular plate, Berry *et al.* have made a significant remark that the radiation mechanism strongly depends on the boundary condition of the plate [1]. Another important aspect is that energy loss occurs in the reflection of bending waves at the elastic supported edges, which reduces the radiation from modal vibrations of the plate [2]. These are why modeling of the elastic boundary support is crucial for simulating accurate sound transmission loss of plate-like structures.

The elastic boundary support has been usually modeled with mechanical and moment impedances, but it is not yet well established how to determine the impedances. Several papers have dedicated to investigate the effect of translational and rotational restraint on natural frequencies of finite plates (e.g.[3]), where the analysis was performed with assuming lumped constants of stiffness, inertance and resistance for the impedance boundary condition. However, it is not clear to what extent this lumped model is applicable. Besides, input parameters of the boundary impedances are often experimentally determined by excitation tests. The total loss factor (TLF) measurement by reverberation method is one of the most common measurement [4]. However, the measured value has not been investigated in terms of the discrepancy from the theoretical value.

Focusing on a thin plate supported by an elastic material with a rectangular cross section, this paper is dedicated to improve the usability of the impedance boundary modeling. In Sect. 2, the random-incidence vibration absorption coefficient on the support edge is theoretically formed under the semi-infinite plate terminated by the equivalent mechanical and moment impedances. Subsequently, in Sect. 3, finite element analysis is performed on the impedance model and a precise support material model in order to clarify the reliable condition of the impedance boundary modeling. Finally, the numerical and experimental measurement of the total loss factor is conducted in Sect. 4 and Sect. 5.

## 2 THEORICAL ANALYSIS

### 2.1 Governing Equation

A flat plate is assumed to lie on the $x-y$ plane of the Cartesian coordinate. $e^{j\omega t}$ is assumed as the time convention throughout this paper. The time-harmonic equation of the Kirchhoff-Love thin plate vibration theory is given as

$$B\nabla^2\nabla^2 w - \rho_\mathrm{p}\omega^2 w = f_z + z\frac{\partial f_x}{\partial x} + z\frac{\partial f_y}{\partial y} \tag{1}$$

where $\nabla^2$ is the Laplace operator, $w$ is the out-of-plane displacement, $B$ and $\rho_p$ are the flexural rigidity and the area density of the plate. $B$ is given by $B = E_\mathrm{p}t_\mathrm{p}^3/[12(1-\mu^2)]$, where $E_\mathrm{p}$, $\mu$ and $t_\mathrm{p}$ are the Young's modulus, the Poisson's ratio and the thickness of the plate, respectively. $f_x$, $f_y$ and $f_z$ are the external stress acting on the plate surface in each direction. $z$ is the signed distance from the mid-plane of the plate, which is $t_\mathrm{p}/2$ on the upper face and $-t_\mathrm{p}/2$ on the bottom face, respectively. The relation between the bending-torsional moments and the displacement is described as follows.

$$M_{\alpha\beta} = -B\left[(1-\nu)\frac{\partial^2 w}{\partial\alpha\partial\beta} + \delta_{\alpha,\beta}\nu\nabla^2 w\right] \tag{2}$$

where $\alpha$ and $\beta$ take $x$ or $y$. $\delta_{\alpha,\beta}$ is the component of the unit tensor. Throughout this paper, the internal loss factor of the plate, $\eta_\mathrm{p}$, is set as zero in order to focus on the effect of the edge damping.

### 2.2 Impedance boundary conditions

As Eq. (1) is the partial differential equation of fourth order, two conditions should be defined at a boundary: one is for translational motion and the other is for rotational motion. Assuming the local reactive boundary, these conditions can be generally described by using the mechanical and moment impedances, $Z_\mathrm{Q}$ and $Z_\mathrm{M}$, as follows.

$$\tilde{Q} = \left(\frac{\partial M_\mathrm{n}}{\partial n} + 2\frac{\partial M_\mathrm{s}}{\partial s}\right) = -j\omega Z_\mathrm{Q} w, \qquad M_\mathrm{n} = j\omega Z_\mathrm{M}\frac{\partial w}{\partial n}, \tag{3}$$

where $\tilde{Q}$, $M_\mathrm{n}$, and $M_\mathrm{s}$ are the effective shear force, normal and torsional moments along the boundary, respectively. $\partial/\partial n$ and $\partial/\partial s$ are the normal and tangential directional derivative along the boundary, respectively.

### 2.3 Oblique-incidence reflection coefficient

As depicted in Fig. 1, let us consider a situation where the plane propagative bending wave impinges to the boundary of $x = 0$ at an incidence angle of $\theta$. In this semi-near field, general solution of the Eq. (1) is given

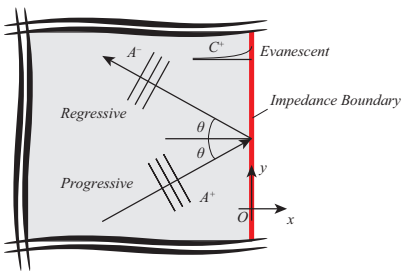


Figure 1. Problem setting for the analysis of the plate bending wave reflection from the impedance boundary

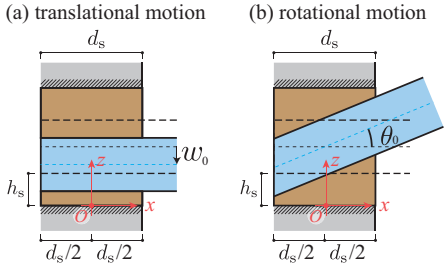


Figure 2. Assumed deformations of a rectangular support material for (a) translational and (b) rotational motions.

as [5]

$$w(x,y) = (A^+ e^{-j\omega k_{Bx} x} + A^- e^{j\omega k_{Bx} x} + C^+ e^{-\omega k_{Bx} x}) e^{-jk_{By} y}, \tag{4}$$

where $k_{Bx} = k_B \cos\theta$, $k_{By} = k_B \sin\theta$ and $k_{Ex} = k_B(1+\sin 2\theta)^{1/2}$. $k_B$ is the bending wave number on the plate defined as $k_B = \omega^{1/2}(B/\rho_p)^{1/4}$. Substituting Eqs. (2) and (4) into the former or latter equation of Eq. (3), the following relations are obtained.

$$\begin{aligned}(\gamma_-\beta_+ - z_q)A^+ - (\gamma_-\beta_+ + z_q)A^- - (j\gamma_+\beta_- + z_q)C^+ &= 0, &(5)\\ (\beta_- - z_m\gamma_-)A^+ + (\beta_- + z_m\gamma_-)A^- - (\beta_+ + jz_m\gamma_+)C^+ &= 0, &(6)\end{aligned}$$

where $z_q, z_m$ are the normalized mechanical impedance and moment impedance defined as $z_q = \omega Z_Q/(k_B^3 B), z_m = \omega Z_M/(k_B B)$, respectively. And the following values are introduced, $\beta_\pm = 1 \pm (1-\nu)\sin 2\theta$ and $\gamma_\pm = (1 \pm \sin 2\theta)^{1/2}$. Combining Eqs.(5) and (6), the oblique-incidence reflection coefficient is obtained as

$$r(\theta) = \frac{A^-}{A^+} = \frac{\gamma_-\beta_+^2 - 2z_+\gamma_- z_q z_m - j\gamma_+(\beta_-^2 + z_q z_m - 2\gamma_- z_m)}{\gamma_-\beta_+^2 + 2z_q + \gamma_- z_q z_m + j\gamma_+(\beta_-^2 + z_q z_m + 2\gamma_- z_m)}. \tag{7}$$

Furthermore, oblique-incidence vibration absorption coefficient is given as $\alpha(\theta) = 1 - |r(\theta)|^2$.

### 2.4 Equivalent impedances of a rectangular elastic support material

Let us consider deformations of a rectangular elastic support material as depicted in Fig. 2. The three-dimensional displacements of the support material are continuous to those of the plate on the joining face and fixed at the opposite face. Furthermore, the other faces are under the free support. In order to derive the impedances in the closed form, the following assumptions are introduced:

1. only the one-dimensional longitudinal vibration is excited in the thickness direction of the support material,
2. the translational out-of-plane displacement and the rotational slope of the plate are uniform over the supporting depth.

The validity of the first assumptions is numerically investigated in Sect. 3. The second assumption is considered to be valid when the bending wavelength is sufficiently larger than the supporting depth. Under the first assumption, the longitudinal modal stress in the support material of the lower side is expressed as

$$\sigma_z(x,z) = k_1 \tilde{E}_s w(x) \frac{\cos(k_1 z)}{\sin(k_1 h_s)} \tag{8}$$

where $w(x)$ is the displacement on the joining face. The second assumption states that the displacement is $w(x) = w_0 + \theta_0 x$ with the constant translational displacement $w_0$ and the constant rotational slope $\theta_0$. $h_s$ is the thickness of the support material, $k_1$ is the wave number of the longitudinal wave in the support material, and $\tilde{E}_s$ is the complex Young's modulus defined as $\tilde{E}_s = E_s(1+j\eta_s)$ with the loss factor $\eta_s$. For the translational motion, the force on the joining face, $z = h_s$, is obtained by integrating $\sigma(x,h_s)$ over the supporting depth $d_s$, whereas for the rotational motion, the moment on the joining face is obtained by integrating $\sigma(x,h_s) \times x$ over the supporting depth. Considering the reaction forces of the support materials on both sides, the mechanical and moment impedance are obtained as follows.

$$Z_Q = \frac{2\int_{-d_s/2}^{d_s/2} \sigma_z(x,h_s)dx}{j\omega w_0} = \frac{2\rho_s \tilde{c}_1 d_s}{j\tan(\omega h_s/\tilde{c}_1)}, \quad Z_M = \frac{2\int_{-d_s/2}^{d_s/2} \sigma_z(x,h_s)x dx}{j\omega\theta_0} = \frac{\rho_s \tilde{c}_1 d_s^3}{6j\tan(\omega h_s/\tilde{c}_1)} \tag{9}$$

where $\tilde{c}_1$ is the speed of longitudinal wave defined as $\tilde{c}_1 = (\tilde{E}_s/\rho_s)^{1/2}$and $\rho_s$ is the material density of the support material. Under the preceding assumptions, Eq. (9) is equivalent mechanical and moment impedance of the rectangular elastic support material.

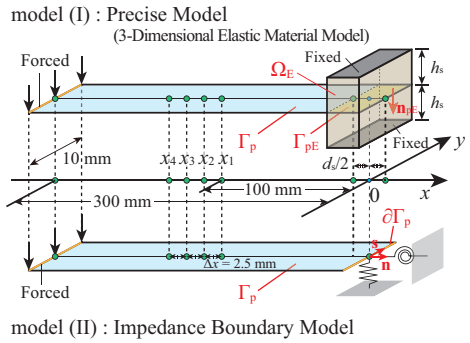


Figure 3. Problem settings and domain notation for calculating mechanical and moment impedances.

Table 1. Physical properties of the plate and supporting material.

| property | plate (glass) | support (putty) |
|---|---|---|
| Young's modulus [N/m$^2$] | $E_p = 7.5 \times 10^{10}$ | $E_s = 1.0 \times 10^6$, $1.0 \times 10^8$ |
| Poisson's Ratio [] | $\nu = 0.22$ | N/A |
| Loss Factor | $\eta_p = 0$ | $\eta_s = 0.5$ |
| Material Density [kg/m$^3$] | $\rho_p/t_p = 2,500$ | $\rho_s = 1,000$ |
| Thickness [m] | $t_p = 0.01$ | $h_s = 0.005$ |
| Depth [m] | N/A | $d_s = 0.015$ |

## 3 NUMERICAL INVESTIGATION

This section discusses the validity of the mechanical and moment impedances given in the previous section through the finite element analysis (FEA). Figure 3 shows the problem setting and the domain notation in this section. The boundary condition of the plate and the elastic material is free support unless otherwise indicated. The physical properties for the calculation are listed in Table 1.

### 3.1 Analysis procedure of normal-incidence vibration indicators

The bending vibration field becomes one-dimensional in the strip plate, which is described as

$$w(x) = A^+ e^{-jk_B x} + A^- e^{jk_B x} + C^+ e^{-k_B x} + C^- e^{k_B x} \tag{10}$$

By observing the displacements at four points, $x_1$ to $x_4$, the following matrix equation can be set according to Eq. (10).

$$\begin{bmatrix} e^{-jk_Bx_1} & e^{jk_Bx_1} & e^{-k_Bx_1} & e^{k_Bx_1} \\ e^{-jk_Bx_2} & e^{jk_Bx_2} & e^{-k_Bx_2} & e^{k_Bx_2} \\ e^{-jk_Bx_3} & e^{jk_Bx_3} & e^{-k_Bx_3} & e^{k_Bx_3} \\ e^{-jk_Bx_4} & e^{jk_Bx_4} & e^{-k_Bx_4} & e^{k_Bx_4} \end{bmatrix} \begin{Bmatrix} A^+ \\ A^- \\ C^+ \\ C^- \end{Bmatrix} = \begin{Bmatrix} w(x_1) \\ w(x_2) \\ w(x_3) \\ w(x_4) \end{Bmatrix} \tag{11}$$

Then, the unknown amplitudes of propagative and evanescent waves, $\{A^+, A^-, C^+, C^-\}^T$, are obtained by solving the above equation. It was confirmed by a preliminary study that the theoretical impedances best approximate those of the precise model (I) just at the middle point of the joining depth: the middle point is set as $x = 0$ as depicted in Fig. 5. Then, normalized mechanical and moment impedances at $x = 0$ and normal-incidence vibration absorption coefficient are calculated as follows:

$$z'_q = \frac{A^+ - A^- + jC^- jC^-}{A^+ - A^- + C^+ + C^-}, \qquad z'_m = \frac{A^+ - A^- - C^- C^-}{A^+ - A^- - jC^+ + jC^-}, \qquad \alpha_n = 1 - \left|\frac{A^-}{A^+}\right|^2.$$

### 3.2 Results and discussions

FEA for the model (I) is performed under shear limp and elastic conditions for the support material. The former condition corresponds to the presented impedance model, and the shear stress is neglected in the FEA. The default physical properties are the same as those investigated in the previous section. Calculation is done at the 1/12 octave center frequency from 16 to 4,000 Hz. The wavelength of the bending wave on the plate at

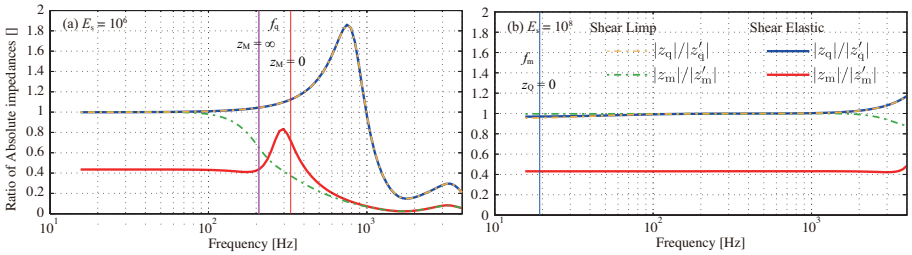


Figure 4. Ratio of the absolute mechanical (moment) impedance of the model (II) to that of the theoretical model. The Young's moduli of the support material are (a) $10^6$ and (b) $10^8$.

4,000 Hz is 0.16 m, and enough larger than $d_s$. Then, the second assumption stated in Sect. 2.4 is acceptable in this point.

Figure 4 shows calculation results: ratio of the absolute impedance of the model (II) to that of the model (I). For the shear limp condition, the theoretical model presented in Sect. 2 well approximates the mechanical and moment impedances around and below $f_q$, the translational mass-spring resonance frequency. Above $f_q$, the support material can no longer be considered as a lumped constant system, which causes the pronounced discrepancy. Regarding the shear elastic model, the mechanical impedance is almost the same as those of the shear limp model. However, the moment impedance is underestimated in the entire frequency range by neglecting the shear stress of the support material. In particular, the ratio is constant below $f_q$. Note that these tendencies are also observed when changing plate thickness and the support material thickness and depth.

## 4 NUMERICAL MODELING OF A TOTAL LOSS FACTOR MEASUREMENT

The TLF measurement by the reverberation method is often performed to get or to estimate input values for theoretical or numerical calculations. However, it is not clear how measured values involve discrepancies from the theoretical values for the diffuse field, which increases the uncertainty of subsequent calculations. In this section, the TLF measurement is numerically modeled to understand the behavior of measured values. This practical information is valuable for experimental verification of the proposed impedance model in future work.

### 4.1 Theoretical foundation

When the 60 dB decay time, $T_{60}$, is measured, a total loss factor $\eta_{tot}$ is obtained as

$$\eta_{tot} = \frac{6 \ln 10}{\omega T_{60}}, \tag{12}$$

because of the definition, $\gamma = \eta_{tot}\omega$, where $\gamma$ is the exponential decay rate.

In the two-dimensional diffuse vibration field, the mean-free path is given as $\pi S/l_{tot}$ with the plate area $S$ and the total perimeter length $l_{tot}$. Then the exponential decay rate, $\gamma_{\mathrm{DF}}$, is defined by $\gamma_{\mathrm{DF}} = c_g l_{tot}\alpha_r/\pi S$, where $c_g$ is the group velocity of the bending wave defined as $c_g = d\omega/dk_B$, and $\alpha_r$ is the vibration absorption coefficient for 2-D random-incidence. Based on these equations, the total loss factor in the diffuse vibration field is theoretically given as

$$\eta_{tot} = \frac{c_g l_{tot}\alpha_r}{\pi\omega S}. \tag{13}$$

### 4.2 Numerical analysis conditions

Following the reference [6], calculation arrangement is set as illustrated in Fig. 5. In the FEA, all perimeters are set as impedance boundaries because this measurement is usually performed for specimens in normal service

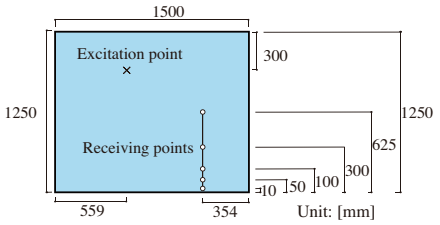


Figure 5. A default geometry for the calculation of the total loss factor.

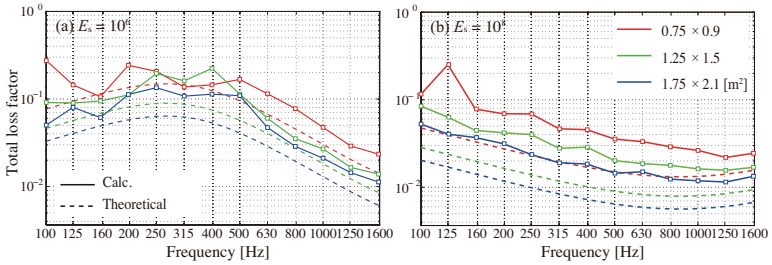


Figure 6. Loss factors calculated for the plate with different sizes and the same aspect ratio. The Young's moduli of the support material are (a) $10^6$ and (b) $10^8$.

condition. The impedance values are given by Eq. (9). Calculation is executed in 0.5 Hz intervals from 0 to 2000 Hz. Subsequently, the transfer function of the acceleration response is converted to the transient response by the inverse Fourier transform. The reverberation time, $T_{60}$, is determined by the least square regression of the energy decay curve obtained by the backward integration of the filtered transient response. The total loss factor is determined by Eq. (12) and the 5-point-average of $T_{60}$. It is well known that the reverberation of the band-pass filter (BPF) itself affects the reverberation time (RT) of the filtered response. In order to approximately equalize the cut-off characteristics among the different bands, the order of the 1/3-octave band FIR filter of the center frequency $f_c$ is set as $N \times 2^M$, where $N$ is the order at 1 kHz and $M$ is calculated by

$$M = \lfloor \log_2(1000/f_c) + 0.5 \rfloor,$$

and in this case, $N = 64$ is appropriate by a preliminary study.

### 4.3 Results and discussions

#### 4.3.1 Effect of the plate size

It is obvious from Eq. (13) that TLF of a vibration system depends on the area and the total perimeter length. The TLF are calculated for three sizes of the plates: 40 % smaller and larger plates than the default size. Figure 6 compares calculated results with the theoretical values for the diffuse vibration field. The calculated results appear to capture the frequency trends of the theoretical values. Furthermore, TLFs for the smaller plate fluctuate more than those for larger plates do. However, the calculated values are two to four times larger than the theoretical values in the entire frequency range. In general, the measurement of the sound absorption coefficient by reverberation room method involves two main error factors that cause the discrepancy from the theoretical value under the diffuse field assumption. One is the lack of the diffusivity, which usually appears as the underestimation of the sound absorption coefficient. The other is the diffraction at the edge of the finite specimen, which usually appears as the overestimation of the sound absorption coefficient. Similarly, the TLF measurement on the rectangular plate involves the non-diffuseness and the diffraction effects, and the latter seems to be predominant. Although all perimeters are impedance boundaries in the present study, the diffraction effect is considered to occur at the plate's corners.

#### 4.3.2 Effect of the support material's properties

Figure 7(a) shows the calculated TLF with changing the support material's loss factor and fixing the Young's modulus to $1.0 \times 10^6$ N/m$^2$. Figure 7(b) shows the calculated TLF with changing the Young's modulus of the support material and fixing the loss factor to 0.5. As discussed in the above, the discrepancy between calculated and theoretical values appears to be large around the mass-spring resonance frequency at which the TLF becomes high. Inverse estimation of the support material's physical parameters or equivalent resistance, stiffness and inertance constants is often performed in order to obtain the input parameters for theoretical and

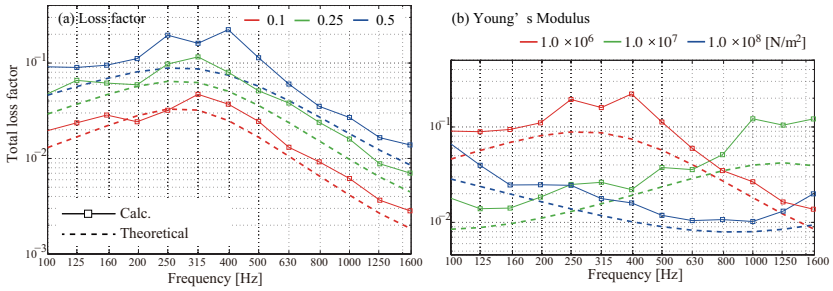


Figure 7. Loss factors calculated with changing the physical property of the seal: (a) loss factor and (b) Young's modulus.

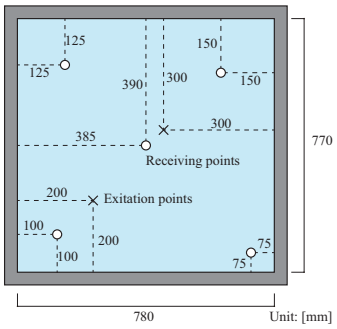


Figure 8. A geometry for the measurement of the total loss factor.

Table 2. The types of the measured window.

| | | |
|---|---|---|
| glass thickness [m] | | |
| | front side | 0.004 |
| | back side | 0.006 |
| thickness of air layer [m] | | 0.002 |
| sash material | | aluminum |

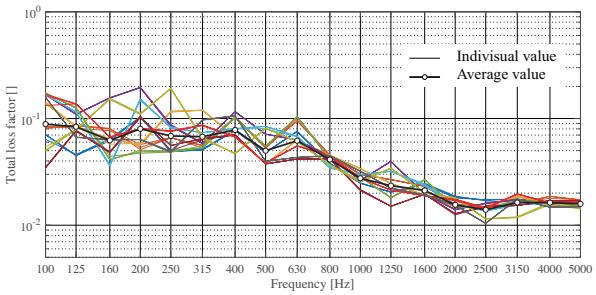


Figure 9. Measured Loss factors on individual excitation and receiving points

numerical calculations [7]. However, from the above observations, the support material's damping parameter such as the loss factor and equivalent resistance constant can be overestimated.

## 5 EXPERIMENTAL MEASUREMENT OF THE TOTAL LOSS FACTOR

In the previous sections, it is clarified how different the measured value is from the theoretical one. Following that, this section reports the results of TLF measurement of a real window system.

### 5.1 Measurement conditions

Figure 8 and Table 2 demonstrate the set-up of the measurement. We arranged double pane windows for certain reasons, although the glass plate with supporting putty is investigated assuming a single pane window in the previous section. Also, the physical property of the windows is not clear as the reason for the difficulty of measurement. Therefore, the purpose of this section is following the tendency of measured values. In this measurement, two excitation points and five receiving points are set, and each measurement is repeated three times. The windows are excited by dropping a steel ball of 20 mm diameter 100 mm above the window, and this vibration is measured by an acceleration pickup at five receiving points. Finally, the total loss factor of windows is determined by measured $T_{60}$ by averaging the measurements of 30 times and Eq. (12). Note that the taps of the FIR filter are set as $128 \times 2^M$ by preliminary analysis. Measurement is analyzed at the 1/3 octave bands from 100 to 5000 Hz.

### 5.2 results and discussions

Figure 9 shows measured TLF by individual measurement and its averaging value. Results on same excitation and receiving points are illustrated by the same color. While the measured values of TLF at the same condition are very close in the entire frequency range, the ones on different conditions vary widely in low frequencies. However, estimating the equivalent impedance can be enable based on this result, and it can lead to accurate simulation of the sound transmission loss.

## 6 CONCLUSION

In this paper, mechanical and moment impedances of a rectangular supporting elastic material were derived in closed form with the some assumptions. Theoretical analysis was provided to investigate the behaviors of bending wave absorption at the impedance boundary. Incidence angle dependency of the vibration absorption coefficient was confirmed to be weak until about 60-degree-incidence. The proposed impedances were compared with those of the precise support material model by the finite element analysis. This study confirmed that the presented mechanical impedance agreed well with the precise model around and below the translational mass-spring resonance frequency. On the other hand, the presented moment impedance was underestimated in entire frequency range due to neglecting the shear reaction of the support material. Furthermore, above the translational mass-spring resonance frequency, the support material can no longer be replaced as a lumped constant system. Thus the impedance boundary model does not sufficiently simulate the behavior of the precise model in particular at high frequencies.

Numerical modeling of the loss factor measurement was performed in order to investigate the difference between the theoretical and measured values. Compared with the theoretical TLF under the diffuse field assumption, the calculated values were overestimated due to the diffraction effect and the self-reverberation of the band pass filter. This tendency should be kept in mind when conducting inverse estimation of the support material's physical parameters or equivalent resistance, stiffness and inertance constants.

Finally, experimental measurement is executed. Although this condition widely differs from numerical measurement in Sect 4, the result implies the numerical measurement corresponds to the experimental ones.

## REFERENCES


[1] Berry, A; Guyader, J. L; Nocolas, J. A general formulation for the sound radiation from rectangular baffled plate with arbitrary boundary conditions, Journal of Acoustics Society of America, Vol 88 (6), 1990, 2792-2802.

[2] Sakuma, T; Egawa, K; Yasuda, Y. Numerical analysis of sound transmission loss of glass pane – On the treatment of edge damping, Proceedings of Inter-Noise 2008, Shanghai, China, October 26-29, 2008, No.0486.

[3] Leissa, A. W. Vibration of Plates, Acoustical Society of America, 1993.

[4] Heckl, M. Measurements of absorption coefficients on plates, Journal of Acoustics Society of America, Vol 34 (6), 803-808, 1962.

[5] Cremer, L; Heckl, M; Petersson, B. A. T. Structure-borne sound, Springer, 3rd edition, 2004.

[6] Yoshimura, J; Sugie, S; Toyoda, E. Effects of size and edge damping on measurement results for sound reduction index of glass pane, Proceedings of Inter-Noise 2006, Honolulu, America, December 3-6, 2006, No.641.

[7] Asakura, T; Sakamoto, S. Study on the absorptive boundary condition of elastic plate in bending wave analysis, Proceedings of Annual Meeting on Environmental Engineering (Architectural Institution of Japan), 233-234, 2008.